Blue Economy

Volume 2 | Issue 2 Article 3

2024

Synthesis and Characterization of UiO-66-NH2 (Zr) Metal–Organic Frameworks: Chitosan and its aminated derivatives to remove toxic Cr (VI) from Industrial Wastewater

Bassma M. Ali
College of Pharmacy, Arab Academy for Science, Technology and Maritime Transport, Abu-Qir, Alexandria, Egypt

Zainab Ali
Medical research institute, Alexandria University, Alexandria, Egypt

Elen Emad
College of Pharmacy, Arab Academy for Science, Technology and Maritime Transport, Abu-Qir, Alexandria, Egypt, ellinemadyouseef@aast.edu

Ragaa Ahmed
Maritime Postgraduate Studies Institute, Arab Academy for Science, Technology and Maritime Transport, Abu-Qir, Alexandria, Egypt

Ayat Khasawneh
Water and Environmental Engineering Department, Al-Balqa' Applied University, P.O. Box 50, Al-Huson, Irbid, Jordan

ISSN: 2805-2986 — e-ISSN: 2805-2994

See next page for additional authors

Synthesis and Characterization of UiO-66-NH2 (Zr) Metal–Organic Frameworks: Chitosan and its aminated derivatives to remove toxic Cr (VI) from Industrial Wastewater

Authors

Bassma M. Ali, Zainab Ali, Elen Emad, Ragaa Ahmed, Ayat Khasawneh, Khalideh Al bkoor Alrawashdeh, Rebhi A. Damseh, Jalal A. Al-Tabbal, Kamel K. Al-Zboon, Petros Samaras, Yasser Dessouky, and Kareem Tonbol

RESEARCH ARTICLE

Synthesis and Characterization of UiO-66-NH_2 (Zr) Metal−organic Frameworks: Chitosan and Its Aminated Derivatives to Remove Toxic Cr (VI) From Industrial Wastewater

Bassma M. Ali [a], Zainab Ali [b], Elen E. Youssef [a,*], Ragaa Ahmed [c], Ayat Khasawneh [d], Khalideh A.B. Alrawashdeh [e], Rebhi A. Damseh [e], Jalal A. Al-Tabbal [f], Kamel K. Al-Zboon [d], Petros Samaras [g], Yasser Dessouky [h], Kareem Tonbol [i]

[a] College of Pharmacy, Arab Academy for Science, Technology and Maritime Transport, Abu-Qir, Alexandria, Egypt
[b] Medical Research Institute, Alexandria University, Alexandria, Egypt
[c] Maritime Postgraduate Studies Institute, Arab Academy for Science, Technology and Maritime Transport, Abu-Qir, Alexandria, Egypt
[d] Water and Environmental Engineering Department, Al-Balqa' Applied University, P.O. Box 50, Al-Huson, 19117 Irbid, Jordan
[e] Mechanical Engineering Department, Al-Huson University College, Al-Balqa' Applied University, P.O. Box 50, Al-Huson, 19117, Irbid, Jordan
[f] Applied Science, Al-Huson University College, Al-Balqa Applied University, Al-Huson, Jordan
[g] Department of Food Science and Technology, International Hellenic University, Thessaloniki, Greece
[h] College of Engineering and Technology, Arab Academy for Science, Technology and Maritime Transport, Abu-Qir, Alexandria, Egypt
[i] College of Maritime Transport and Technology, Arab Academy for Science, Technology and Maritime Transport, Abu-Qir, Alexandria, Egypt

Abstract

This study used adsorbent hydrogel beads on chitosan (CS) coated with the commercially prepared metal−organic framework and its aminated derivative to chromium (VI) ions from their aqueous solutions. Higher removal (%) and higher adsorption capacity values were recorded using CS and its aminated derivatives, UiO-66-NH_2 (Zr) (0.5% CS) adsorbent (87% and 95 mg/g, respectively) compared with those using the CS adsorbent (86% and 93 mg/g using 1% CS); contact time was 180 min, with maximum removal (%) reaching 87% and maximum adsorption capacity of 95 mg/g. The pH of the studied medium was in the range of 1−8. It was found that the maximum values of removal (%) and adsorption capacity values were observed at pH 2, and the Cr (VI) concentration was studied in the range of 10−200 ppm. The highest removal (%) was about 100% using 10 and 25 ppm of Cr (VI), while the maximum adsorption capacity was found to be 132 mg/g and was recorded using 200 ppm of Cr (VI). Adsorption experiments at 150 rpm were conducted to record maximum adsorption capacity and higher removal (%) values. The developed adsorbent demonstrated good adsorption properties, with removal exceeding 60% after six cycles and a maximum capacity of 52 mg/g. In conclusion, the metal−organic framework/CS adsorbent beads have the potential to be a novel and effective large-scale adsorbent for the removal of hazardous Cr (VI) ions from industrial effluents.

Keywords: Aminated chitosan, Conservation, Cr (VI) hexavalent chromium, Land, Metal−organic framework, Wastewater, Water

Received 30 June 2024; revised 21 July 2024; accepted 22 July 2024.
Available online 23 September 2024

* Corresponding author at: College of Pharmacy, Arab Academy for Science, Technology and Maritime Transport, Abu-Qir, Alexandria, 21648, Egypt.
E-mail address: ellinemadyouseef@egypt.aast.edu (E.E. Youssef).

https://doi.org/10.57241/2805-2994.1028

1. Introduction

Water is the most essential source of life on earth; 97% of the water belongs to the ocean, while only 1% may be controlled and exploited. Fast industrialization, increasing urbanization, growing population, and unregulated use of natural resources are inflicting permanent harm to the ecosystem (Bashir *et al.*, 2023). Water pollution is one of the most serious environmental issues, owing to the continuous release of large quantities of contaminants into the environment, such as toxic heavy metal ions. Numerous heavy metals and synthetic organic substances are among the more dangerous industrial pollutants. But once more, in high enough doses, they could pose serious risks to marine life and human health (Lou *et al.*, 2023).

Water shortages in developing nations, coupled with population growth, droughts, health regulations, and competing demands, pose challenges to meeting the global demand for clean and safe water (Yoo *et al.*, 2023). Industrial wastewater contains toxic pollutants such as acids, bases, toxic materials, and suspended solids, as well as surfactants, emulsifiers, petroleum hydrocarbons, and trace amounts of heavy metals (Amir Afshar and Ghaee, 2016).

The three most prevalent types of water pollution are heavy metals, herbicides, and microbes. Numerous heavy metals and synthetic organic substances are among the more dangerous industrial pollutants. But once more, in high enough doses, they could pose serious risks to marine life and human health (Lou *et al.*, 2023). Toxic heavy metal ions in industrial effluent, including Cr (VI), Ni (II), and Cu (II), have raised environmental issues. Due to the ability of biomagnification, these devastating metal ions are harmful in high amounts. Cr (VI) is a high-priority hazardous heavy metal due to its mutagenesis and carcinogenic properties (Wang *et al.*, 2016a, 2016b).

The behavior of metals is influenced by the oxidation state of heavy metal ions. Chromium, a chemical element that commonly exists in two stable oxidation states, namely Cr (III) and Cr (IV), is frequently detected as a pollutant in industrial water originating from various sectors such as electroplating, paint, tanning, pigment production, and metallurgy (VI). Moreover, it is widely recognized that although hexavalent chromium (Cr (VI)) is soluble and poses a threat to human health, trivalent chromium (Cr (III)) is considered a crucial micronutrient for the metabolic processes of humans, plants, and animals. Chromium atoms are predominantly observed in chromate and cationic complexes within natural water systems (Prasad *et al.*, 2021).

When these ions are present in large quantities, they can pose significant environmental and health risks. The ions have a tendency to trap in the metal–organic framework (MOF) structure, form interactions with or replace the existing metal ions, and are therefore detected. That is why an efficient approach for detecting very low concentrations of transition-metal cations is always required (Shafqat *et al.*, 2023).

Heavy metal ions have been removed using chemical, physical, and biological processes, including ion exchange, chemical precipitation, reverse osmosis, bioremediation, membrane filtration, flocculation, ozonation, sedimentation, adsorption, and photocatalysis, among the methods used to reduce water pollution. Researchers do not consider procedures such as coagulation, flocculation, ion exchange, and membrane filtration to be useful due to major drawbacks such as large sludge volumes and high costs (Bashir *et al.*, 2023).

Over the last two decades, photocatalysis and adsorption have been regarded as promising methods for the removal of water pollutants. Adsorption is an efficient and cost-effective method. Traditional adsorbents, such as activated carbon and chitosan (CS), have limited adsorption capabilities and efficiency. New potential adsorbents are desperately required (Ihsanullah *et al.*, 2016).

Smart hydrogels are intensively explored in biological and material domains for their adaptability, responsiveness, and biocompatibility. Although the gelator types differ, their mechanisms of action are mostly the same; they form a 3D network in response to a specific trigger, such as heat, radiation, or chemical stimuli. The unique stimulus response enables their use in various areas and situations, including active pharmaceutical ingredient distribution in multicomponent drug delivery systems (Shriky *et al.*, 2022).

CS has gained popularity in recent years due to its lower cost compared with activated carbon. The structure contains amino (-NH_2) and hydroxy (-OH) groups. These active sites remove heavy metals from wastewater. CS has been changed by physical, chemical, and hybrid approaches to improve its ability to adsorb heavy metals (Wang *et al.*, 2016a, 2016b).

MOFs are a group of compounds that have gained attention in recent times. These compounds are formed by coordinating metal ions or clusters with organic ligands, resulting in the creation of structures that can be one-dimensional, two-dimensional, or

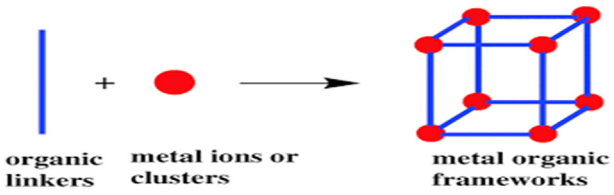

Fig. 1. Schematic preparation of a metal–organic framework (Abdelrazik et al., 2016).

three-dimensional as shown in Fig. 1. Porous coordination polymers are a distinct subset of coordination polymers that are notable for their frequent possession of pores. Their exceptional porosity, tunability, and chemical versatility have established them as a viable option for a diverse array of applications, such as gas storage, catalysis, drug delivery, and notably wastewater treatment (Shafqat *et al.*, 2023).

The adaptability and adjustability of MOFs render them notably pertinent for tackling the distinct contaminants present in industrial effluents. It is possible to tailor the organic ligands present in MOFs to exhibit selective affinity toward heavy metals and organic compounds, thereby facilitating their precise and efficient removal from the environment. As an illustration, MOFs featuring ligands containing sulfur have exhibited a notable propensity for binding heavy metals, including lead and mercury. Conversely, MOFs containing polar or aromatic ligands have demonstrated potential for the sequestration and decomposition of diverse organic contaminants. Hence, through meticulous selection of MOF constituents, it could be feasible to devise customized remedies for the management of industrial effluents (Garg *et al.*, 2023).

Motivated by the advantages of MOFs, we developed METAL MOF/AmCHITOSAN beads as a low-cost adsorbent to remove Cr (VI) from industrial wastewater and examined the reusability of the developed MOF/aminated chitosan (AmCS) adsorbent.

2. Materials and methods

2.1. Materials

From the leftovers of shellfish eateries in Alexandria, Egypt, shrimp shells were gathered. The shipment of sodium hydrogel (medium consistency) came from Sigma-Aldrich Telangana, 500018, India. Sigma-Aldrich was used to supply acetic vinegar (purity 99.8%) and ethylene diamine (Germany). Potassium dichromate ($K_2Cr_2O_7$) was bought from Aladdin Industrial Corporation Suite 601, Shanda Building, No. 196 xinjinqiao Road, Pudong District, Shanghai 201206, China, and calcium chloride (anhydrous, 90%) was purchased from Fisher Scientific in Fair Lawn, New Jersey, USA. By dissolving a suitable amount of the analytical reagent $K_2Cr_2O_7$ in 1000 ml of deionized water, a stock solution of Cr (VI) (1000 mg/l) was created. El Nasr Pharmaceutical Chemicals Company Oubour, Qalyubia, Egypt. provided sodium hydroxide and hydrochloric acid with a concentration range of 30–34%, Egypt. In addition, Sinopharm Chemical Reagent Co. Ltd. in Germany provided the 1,5-diphenylcarbazide. In addition, absolute ethanol, formic acid, acetic acid, and dimethylformamide were produced. Formic acid, oleic acid, formic chloride, methanol, ethanol, and potassium hydroxides were purchased from Sinopharm Chemical 99 Reagent Co., Building 1, No.801, Hutai Road, Jing'an District Shanghai, Shanghai, 200002 China and used as received.

2.1.1. Preparation of chitosan

According to the reported deacetylation method, CS was prepared from the extracted chitin (Mosquera, 2013). Chitin was soaked in a solution of 50% NaOH for 12 h at 100–120 °C. The excess NaOH was removed by washing the obtained CS many times using double distilled water.

2.2. Preparation of aminated chitosan

AmCS is a derivative of CS, prepared and purified according to previously published work (Wang *et al.*, 2013). First, chitin (4 g) was activated using 50 ml of 4 m mol of p-benzoquinone (PBQ) as a coupling agent at a pH of 11. The reaction mixture was conducted under stirring for 4 h at 50 °C. PBQ-activated chitin was collected and washed several times to remove the unreacted PBQ to ensure the safety of activated chitin. Next, the activated chitin was soaked in 50 ml of ethylene diamine solution (1.8 mm) at 50 °C for 6 h. The resultant aminated chitin was separated and washed many times with water to remove the unreacted substances (Nirmal Kumar and Oommen, 2012). Finally, AmCS was obtained by deacetylation of the aminated chitin using a solution of 50% NaOH for 6 h at 100–120 °C. The produced AmCs were purified and washed many times with distilled water to remove the excess NaOH until the pH reached 7, followed by drying at 40 °C (Kumari *et al.*, 2016).

2.3. Preparation of metal–organic form

The selection of UIO-66-type structural materials was based on their superior activity, thermal stability, and reusability, making them a practical

choice for the production of biodiesel (Cavka *et al.*, 2008). In an experimental and theoretical investigation of the reaction between levulinic acid and ethanol to generate biodiesel, Tambat *et al.* (2018) conducted a comparison between UiO-66 (Zr) and UiO-66 (Zr)–NH_2. Previous studies have demonstrated the enhanced performance of UiO-66 (Zr)–NH_2 in comparison to UiO-66 (Zr) by virtue of its dual activation mechanism involving both amino groups (Brnsted base site) and zirconium centers (Tambat *et al.*, 2018). The authors prepared UiO-66 (Zr) and UiO-66 (Zr)–NH_2 using the conventional method and used them for the esterification of various fatty acids with different alcohols, using Lewis's acid site.

2.4. Characterizations

2.4.1. Fourier transform infrared spectroscopy

UiO-66(Zr)–NH_2-, MOF/CS, CS, and MOF/AmCs beads were analyzed by Fourier transform infrared spectroscopy in the wavenumber range of 4000 –450 cm^{-1}. First, characterization was carried out in solid state using potassium bromide (KBr) pellets. Next, the samples were ground in a mortar and homogenized with KBr. Finally, the mixture was pressed in a hydraulic press to cast pellets to a thin thickness; then, a spectrophotometer (Shimadzu FTIR-8400S, Japan) was used for Fourier transform infrared spectroscopy studies.

2.4.2. Thermogravimetric analysis

Using a thermogravimetric analyzer (Model 50/50H; Shimadzu) and a nitrogen atmosphere (30 ml/min), the thermal behavior of the produced dry beads was investigated. At a rate of 10 °C/min, samples were heated from room temperature to 600 °C (Zafar *et al.*, 2022).

2.4.3. Scanning electron microscopy

The surface morphology changes of the prepared dry beads were investigated using scanning electron microscopy (SEM) (JOEL JSM-6360 LA; Hitachi, Japan). First, samples were coated under vacuum with a thin layer of gold before the examination to increase the conductivity of the electron beam, and then introduced into equipment on their holder; after that, equipment parameters, such as accelerated voltage, focusing, and working distance, were adjusted for every sample to get the best images.

2.4.4. Determination of ion-exchange capacity

The amount of amine on the surface of activated hydrogel beads was measured using the published method (Ngah and Fatinathan, 2010); this was done by measuring the beads' ion-exchange capacity (IEC). Crushed samples of MOF/CS and MOF/AmCs with various CS and AmCs amounts were added to a 0.1 M H_2SO_4 solution. After filtering and 12 h at room temperature, the mixture was titrated against a normal NaOH solution (0.1 M). A control titration without the inclusion of a sample was also carried out. IEC was intended to use the following equation:

$$IEC(meq/g) = \frac{(V_2 - V_1)N}{w} \quad (1)$$

The volumes of NaOH required for complete neutralization of H_2SO_4 in the absence and presence of the tested sample are represented by V_1 and V_2, respectively. The variable N denotes the normality of the sodium hydroxide solution, while W represents the weight of the sample in grams.

2.5. Adsorption evaluation experiments

2.5.1. Batch adsorption experiments

Initially, a stock solution of Cr (VI) was prepared by dissolving $K_2Cr_2O_7$ in distilled water, resulting in a final concentration of mg/l. Subsequently, batch tests (10–200 ppm) were conducted by introducing dried sample beads of MOF, MOF/CS, and MOF/AmCS (0.025–0.3 g) into 100 ml of Cr (VI) solution. The adsorption process was conducted using a Lab Companion model SI-300R shaking water bath, with temperatures ranging from 25 to 55 °C and a shaking rate of 25–200 rpm. The pH of the Cr (VI) solution was altered to a range of 1–8 by using 0.1 M solutions of HCl and NaOH. The samples were systematically collected and subjected to filtration at regular time intervals of 15, 30, 60, 120, 180, 240, and 300 min. Subsequently, the filtrate was scrutinized for the presence of any residual Cr (VI) ions. Conversely, the concentration of Cr (VI) ions was determined by measuring the optical density of the purple complex formed with 1,5-diphenylcarbazide at 540 nm using a UV spectrophotometer (Jasco V-530). The subsequent equations may be used to compute the percentage of Cr (VI) removal and the adsorption capacity (q):

$$Removal\% = \frac{Co - Ct}{Co} \times 100 \quad (2)$$

$$q(mg/g) = (Co - Ct) \times \frac{v}{m} \quad (3)$$

where C_o and C_t are the concentrations (ppm; i.e. mg/l) of Cr (VI) at the initial and at time *t*, respectively; *V* is the volume (l) of Cr (VI) solution; and *m* is the mass of adsorbent sample beads (g).

2.6. Adsorption kinetics study

The impact of contact time for adsorption was examined to examine the adsorption kinetics of Cr (VI) on MOFS and the findings.

The capacity increased rapidly in the initial 60 min and the adsorption process reached the equilibrium in 120 min. MOFs are a fascinating class of materials with highly tunable structures and exceptional porosity, making them ideal candidates for adsorption applications. Understanding the mechanism of adsorption onto MOFs is crucial for optimizing their performance and designing them for specific targets. This involves using a combination of adsorption isotherms and kinetic models (Reddy and Lee, 2013).

2.7. Adsorption isotherms

Isotherms describe the relationship between the amount of adsorbate (e.g. metal ions, gas molecules) bound to the MOF surface (qe) and its equilibrium concentration in the solution (Ce) at a constant temperature. Different isotherms represent various adsorption mechanisms, such as Langmuir, Freundlich, and Temkin isotherms (Tambat *et al.*, 2018).

2.8. Reusability experiments

The created beads for eliminating Cr (VI) ions were also created reusable by carrying out the adsorption–desorption procedures.

After the adsorption process was complete, the adsorbent samples were removed from the bulk adsorption runs and soaked in a solution of NaCl (1 M) and ethanol (98%) while being continuously shaken at 250 rpm for 3 h at 25 °C (Bang and Pazirandeh, 1999). Thus, the ability of the bead sample to be reused for Cr (VI) removal was conducted for six consecutive cycles.

3. Results and discussion

3.1. Characterization

3.1.1. Fourier transform infrared spectroscopy analysis

The stretching vibration of the −OH groups was responsible for the broad absorption bands observed at 3446 and 3443 cm^{-1} in both MOF and MOF-CS, as depicted in Fig. 2. In addition, the sample exhibited unique functional groups characterized by COO-stretching, which were observed as a wide, asymmetrical band at 1630 and 1627 cm^{-1}. Moreover, C=C stretching bands were identified at 1410 and 1435 cm^{-1}. Furthermore, it was observed that two peaks of absorption were present in the vicinity of 1062 and 1081 cm^{-1}. In addition, the infrared spectra of CS and AmCS, as shown in Fig. 3, exhibited stretching vibration bands at 3448 and 3000 cm^{-1}, respectively. These bands were attributed to the overlapping stretching vibrations of the OH and NH_2 groups. The modified polymer, AmCS, displays distinct peaks

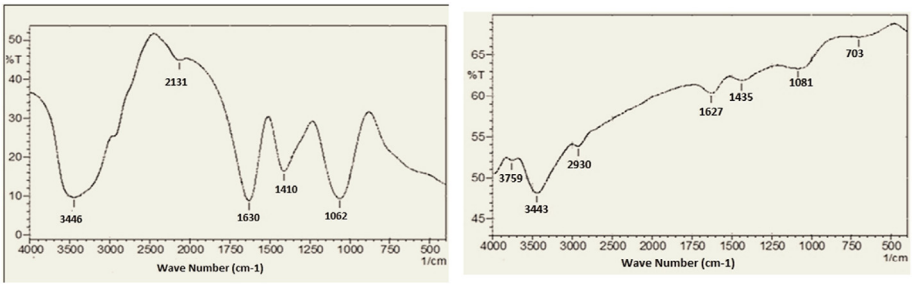

Fig. 2. FTIR spectrum of MOF-activated MOF-CS.

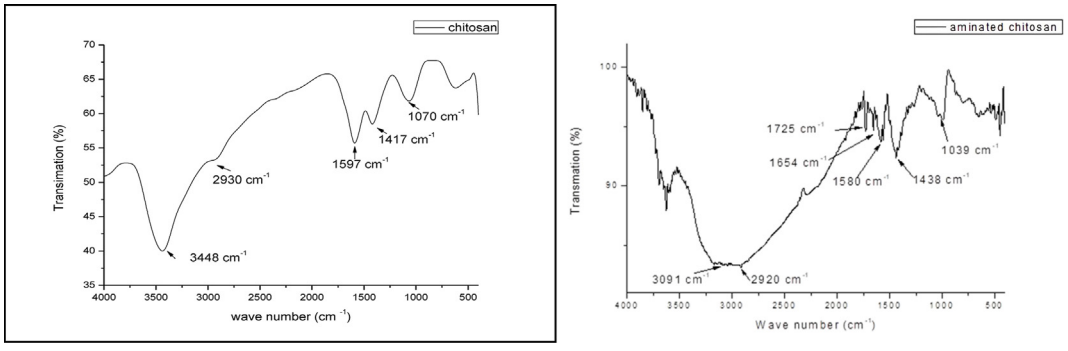

Fig. 3. FTIR spectrum of CS-AmCS.

in these regions that correspond to the augmentation of amine content. The C–H stretching of methyl for CS and AmCS is represented by bands at 2930 and 2920 cm^{-1}, respectively, as illustrated in Fig. 4 by Zabochnicka-Świątek and Krzywonos (2014).

3.2. Thermogravimetric analysis thermographs

Thermal properties of MOF, MOF-PBQ, CS, MOF/CS, and MOF/AmCS chemically cross-linked hydrogel beads were evaluated by the thermogravimetric analyzer in a nitrogen atmosphere at a heating rate of 10 °C/min. It was clear from the figures that the initial weight loss for all samples could be attributed to the small amount of moisture. The weight loss in the case of Alg (Fig. 5) occurs after 98.94 °C at a relatively high rate up to 230 °C, where hydrogel lost about 25% of its original weight. The rate of weight loss slows as the temperature rises above this level. However, in the case of MOF-CS (Fig. 5), a distinct behavior was noticed, most likely as a result of the beads' increased thermal stability when compared with MOF beads. Compared with the MOF beads, the weight reduction at 230 °C has decreased.

Fig. 5 demonstrates the degradation of CS and AmCS under a nitrogen atmosphere. The first weight loss starts from ambient temperature to about 150 °C, which was referred to as imbibing the polymer's water content trapped by its hydrophilic groups (hydroxyl and amine groups). The high moisture content of AmCS (11.15%) compared with CS (7.2%) was attributed to increasing the hydrophilic nature of the modified polymer by the amination process. According to Pawlak and Mucha, the principal destructive decomposition of the CS backbone ranged from 220 °C to 350 °C due to the oxidative decomposition of the pyranose ring. In this stage, the destruction forms cross-linked fragments that decompose at a higher temperature (Niñã *et al.*, 2007).

The results indicated that the thermal stability of CS decreased after the amination process, where CS lost half its weight (T_{50} °C) at 347.2 °C compared with that at 309.4 °C in the case of AmCS. This may be attributed to the role of amine groups in enhancing the thermal degradation process. It can also be anticipated that chemically cross-linked MOF/CS (Fig. 5) and MOF/AmCS (Fig. 5) beads exhibit more thermal stability than native MOF, CS, and AmCS biopolymers. This is due to the presence

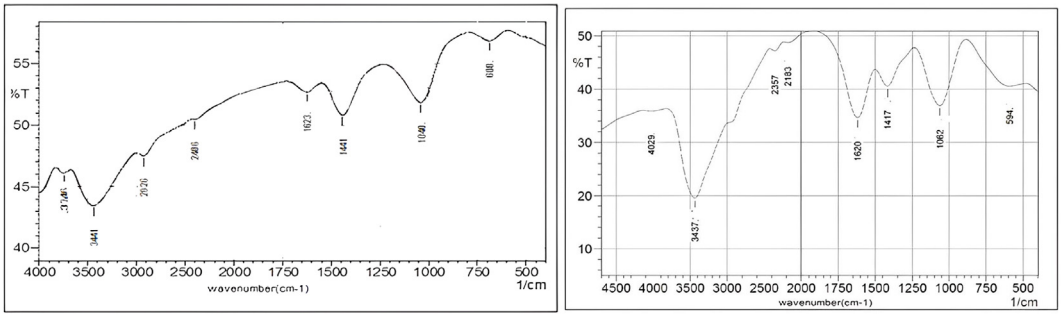

Fig. 4. FT-IR spectrum of MOF/CS beads – MOF/AmCS beads (0.5% AmCS).

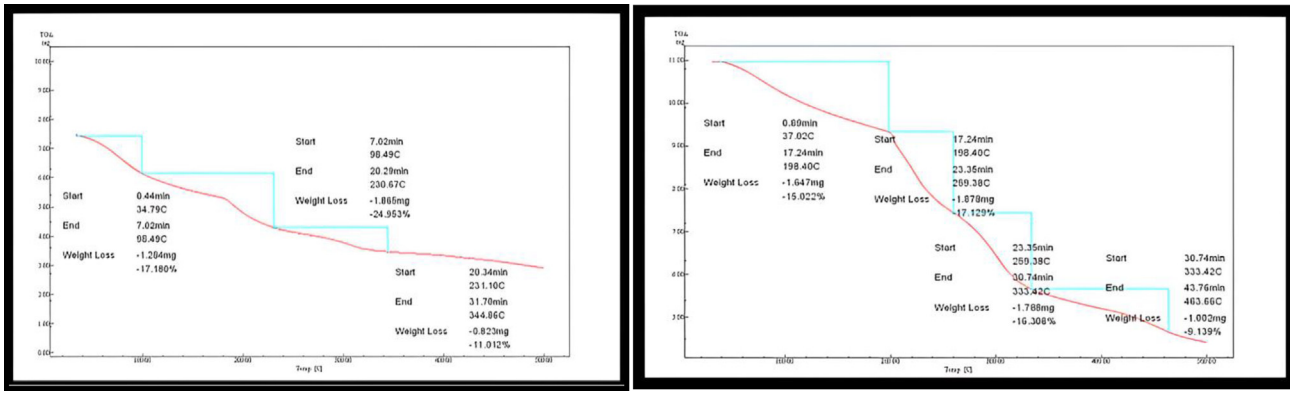

Fig. 5. TGA of MOF and MOF-CS.

of covalent bonds resulting from the coupling process using PBQ, which enhances beads' thermal behavior.

This phenomenon can be explained by consuming part of hydrophilic amine groups in the cross-linking process. It was noticed that the initial weight losses in the case of MOF/AmCS were higher than those in the case of MOF/CS beads, as shown in Table 1. The presence of extra hydrophilic amine groups along the chain backbone facilitates the trapping of moisture molecules into the polymer. In general, it was clear that the chemical modifications improved the thermal stability relative to the parent polymer.

3.3. Scanning electron microscopy analysis

Changes in surface morphology of the prepared dry beads were investigated using SEM. SEM images of MOF, CS, AmCS, and MOF/CS and MOF/AmCS chemically cross-linked hydrogel beads are shown in Figs. 6–9. It was clear that the morphological structure of MOF (Fig. 6) was different than that of the activated MOF with PBQ (Fig. 7), where a granular surface with a small size was observed in the case of MOF, which changed to a curly surface after the activation process by PBQ. However, the surface of CS (Fig. 8) was changed from a granular surface to a smooth surface in the case of AmCS (Fig. 9) after the amination process.

Table 1. TGA data of MOF, CS, AmCS, MOF/CS, and MOF/AmCS chemically cross-linked hydrogel beads (Ninã et al., 2007).

Samples	$T_{50\%}$ (°C)	Weight loss (%) at RT − 150 °C
MOF	315	25.67
Chitosan	347.22	7.2
Aminated chitosan	309.4	11.15
MOF/CS (chemically cross-linked)	489	2.677
MOF/AmCS (chemically cross-linked)	385.1	10.8

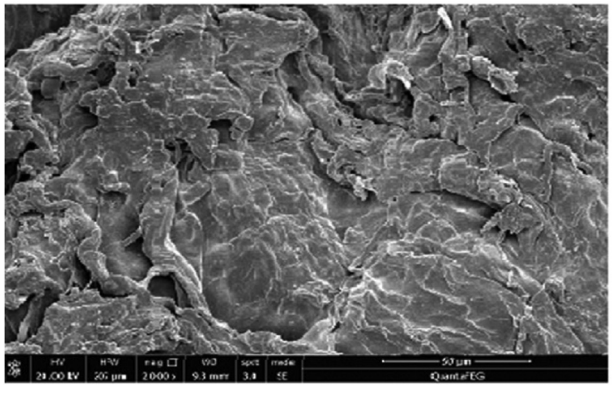

Fig. 6. SEM image of MOF.

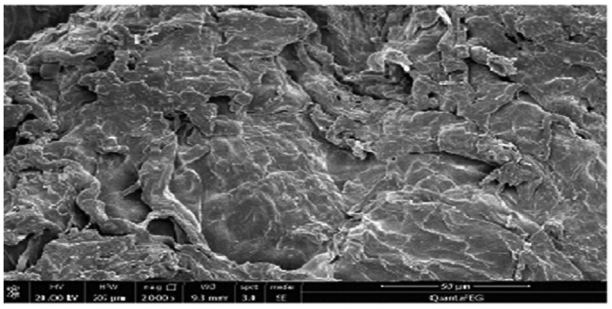

Fig. 7. SEM image of MOF-CS.

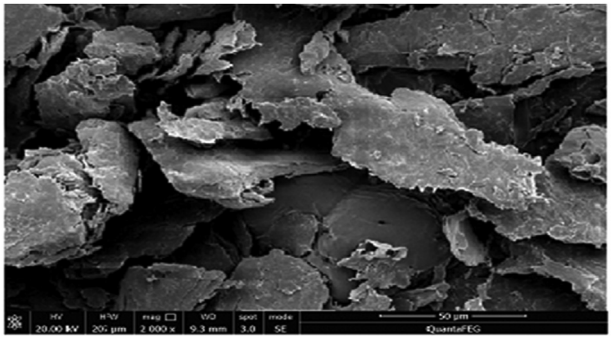

Fig. 8. SEM image of chitosan.

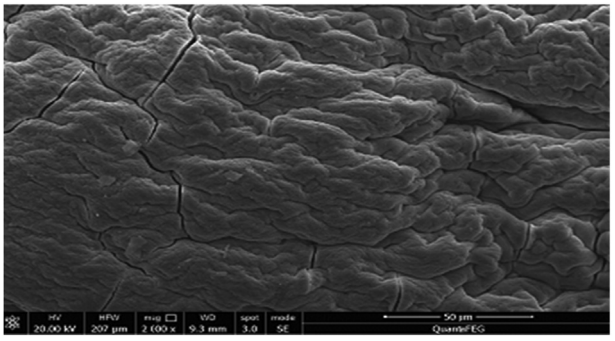

Fig. 9. SEM image of MOF/AmCS (chemically cross-linked) beads.

The bead surface morphology of the developed MOF/CS (Fig. 7) and MOF/AmCS (Fig. 8) was significantly changed compared with native biopolymers, in which a dense and random fibrillar and rougher surface was formed after cross-linking with CS and AmCS. Furthermore, the degree of compaction has been increased obviously in the case of MOF/AmCS compared with that of MOF/CS.

3.4. Ion-exchange capacity determination

Fig. 10 shows the IEC values for different concentrations of CS and AmCS for the chemically

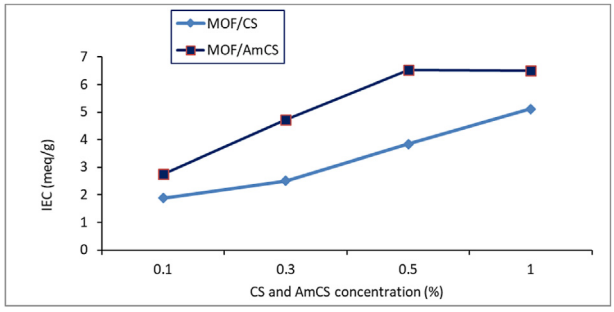

Fig. 10. IEC values for MOF/CS and MOF/AmCS beads.

cross-linked MOF/CS and MOF/AmCS beads that were tested. IEC increased linearly as the CS content rose from 0.1 to 1%, as was observed. However, using 1% CS, it steadily increased from 1.88 mEq/g to a maximum value of 5.12 (mEq/g. In the instance of AmCS, the same behavior was observed, but the maximum IEC value was 6.5 mEq/g using just 0.5% of AmCS. MOF/AmCS IEC values were higher than Alg/CS values in all ratios. This is explained by the additional amine groups that are present on the surface of hydrogel beads compared with CS (produced by AmCS). The IEC values are unaffected by an additional rise in AmCS concentration of up to 1%. The saturation of the majority of active locations with 0.5% of AmCS may help to explain this.

3.5. Swelling studies

The swelling of the desiccated hydrogel beads is mainly caused by the hydration of the present hydrophilic groups of MOFs (OH, COOH), CS (OH and NH_2), and AmCS (OH and excess of NH_2) (Eldin *et al.*, 2012).

Free water molecules enter the network of beads and occupy the rigid pores within the polymer network, increasing the degree of swelling. Fig. 11 illustrates the investigation into the degree of

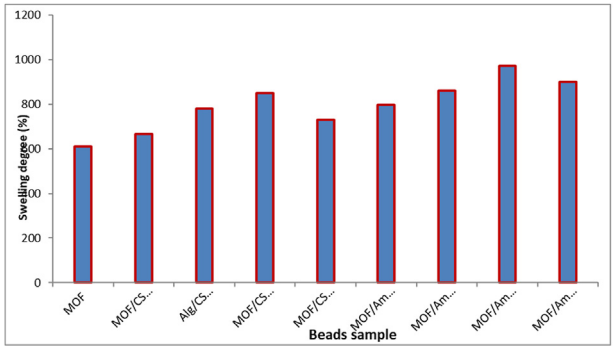

Fig. 11. Swelling degree values for MOF and MOF/CS beads with different concentrations of CS (at constant swelling time of 3 h, room temperature, and 0.1 g sample).

swelling of the produced MOF, MOF/CS, and MOF/AmCS hydrogel beads. It was clear that the swelling degrees of MOF/CS and MOF/AmCS samples were higher than that of MOF beads due to the generated hydrophilic amine groups using CS and AmCS, which impart the hydrophilicity of beads.

Moreover, the swelling degree increased gradually with increasing CS and AmCS concentrations of up to 0.5% and then decreased with further increases of CS and AmCS concentrations of up to 1%. This could be explained by the fact that CS and AmCS are natural hydrophilic polymers, increasing the affinity of water molecules to penetrate the bead network. The molecular chains swell, increasing the number of different amine groups with further increases in AmCS concentrations of up to 1% may produce a very strong ionic interaction with the carboxylate ions of the hydrogel through the formation of a polyelectrolyte complex in addition to the presence of covalent bonds which generated from the chemical cross-linking.

This resulted in a compact and densely networked structure with the minimum swelling degree. These groups do not contribute to the retention of water molecules within the beads. Then the diffusion rate of water molecules is reduced (Al-qudah *et al.*, 2014). From the results, the values of the swelling degree of MOF/AmCS beads were higher than those of MOF/CS beads due to the extra hydrophilic groups generated in AmCS, which enhance the swelling behavior of beads.

3.6. Adsorption evaluation

3.6.1. Effect of CS and AmCS concentrations

The impact of varying concentrations of CS and AmCS on the adsorptive elimination of Cr (VI) was examined under constant adsorption conditions, as depicted in Figs. 12 and 13. These conditions included an adsorbent dose of 0.1 g, a Cr (VI) concentration of 50 ppm/100 ml, a pH of 2, an adsorption temperature of 25 °C, a shaking speed of 150 rpm, and a contact time of 180 min. The results indicate a substantial increase in the removal of Cr (VI) through the use of MOF/CS beads, with removal rates rising from 27 to 86%. Furthermore, the concentrations of CS exhibited an increase from 0.1 to 1% concomitant with the rise in adsorption capacity from 35 to 93 mg/g. The MOF/CS beads have demonstrated an adsorption capacity of 15 mg/g; however, the removal efficiency has been determined to be merely 18%. In contrast, the findings indicate that MOF/AmCS exhibited higher removal (%) and adsorption capacity values compared with MOF/CS beads. The maximum

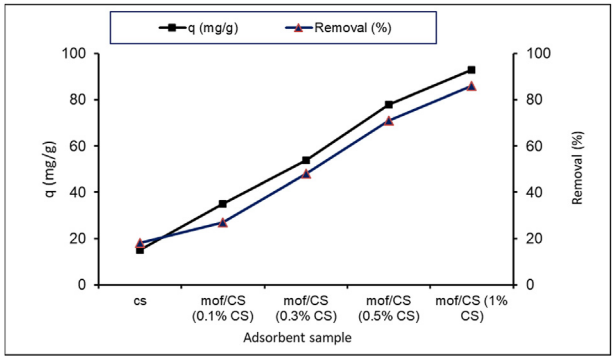

Fig. 12. Effect of CS concentrations on the adsorptive removal of Cr (VI) using MOF/CS beads at a constant adsorbent dose of 0.1 g, Cr (VI) (50 ppm/100/ml), pH = 2, adsorption temperature of 25 °C, shaking speed of 150 rpm, and 180 min as a contact time.

removal achieved using only 0.5% AmCS was 87%, while the maximum adsorption capacity was 95 mg/g.

The observed outcomes could be attributed to the existence of supplementary amine (-NH) clusters on the exterior of MOF/AmCS beads. The cationic amine clusters exhibited remarkable efficacy in eliminating anionic Cr (VI) ions from their respective solutions. After the near-complete adsorption of all Cr (VI) ions through the use of 0.5% of AmCS, any further augmentation in AmCS concentrations beyond the aforementioned percentage did not exert any noteworthy influence on the removal percentage and adsorption capacity. Consequently, Alg/AmCS beads, containing 0.5% AmCS, were deemed suitable for the supplementary batch adsorption investigations.

3.6.2. Effect of contact time

Under controlled conditions, where the adsorbent dose was 0.1 g, the concentration of Cr (VI) was 50 ppm 100/ml, the pH was 2, the adsorption temperature was 25 °C, and the shaking speed was 150 rpm, the impact of contact time (15–300 min) on the removal (%) of Cr (VI), and the adsorption capacity is illustrated in Fig. 14, using Alg/AmCS beads (0.5% AmCS). The results obtained from the study indicate that the extension of contact time from 15 to 180 min resulted in a significant improvement in the removal rate and enhancement of the adsorption process. Consequently, there is a diffusion of a greater number of Cr (VI) ions through the fluid that encompasses the adsorbent particles, leading to a gradual rise in removal efficiency, reaching a maximum of 87% along with a maximum adsorption capacity of 95 mg/g. The adsorption rate of Cr (VI) remained constant even with an extended contact period of up to 300 min, after attaining equilibrium adsorption at 180 min. The depletion of active adsorption sites occurred gradually, resulting in the occupation of said sites by Cr (VI) ions. Consequently, a contact time of 180 min was selected as the optimal duration for adsorption in further batch experiments.

3.6.3. Effect of pH of the medium

The adsorption behavior of Cr (VI) ions is influenced by the pH level of the fluid. The adsorption mechanism of Cr (VI) by MOF/AmCS beads can be elucidated through the application of surface chemistry principles in an aqueous phase. Reddy and Lee (2013) described the remarkable capacity of adsorbents containing amino groups to eliminate Cr (VI) ions from wastewater. In addition, under conditions of solid acidity, the amino (-NH2) groups undergo facile protonation to yield ammonium (-NH3+) moieties, which confer advantageous binding properties toward complex anions including Cr2O72-, CrO42-, and HCrO4-.

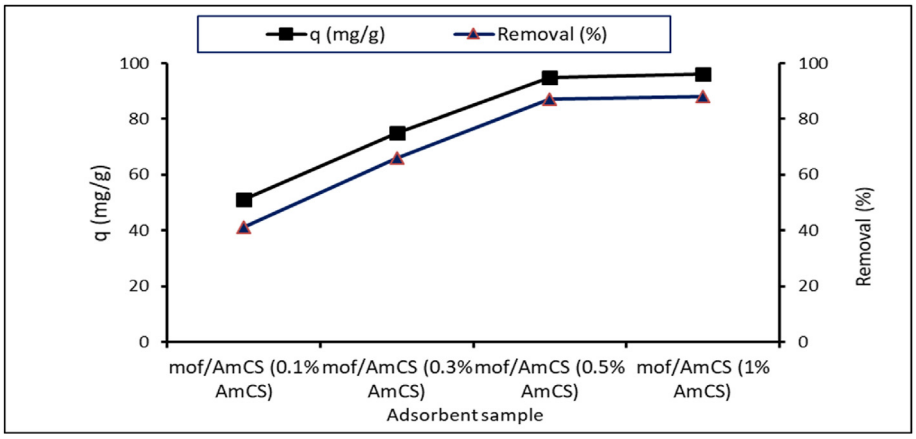

Fig. 13. Effect of AmCS concentrations on the adsorptive removal of Cr (VI) using MOF/AmCS beads at a constant adsorbent dose of 0.1 g, Cr (VI) of 50 ppm 100/ml, pH = 2, adsorption temperature of 25 °C, shaking speed of 150 rpm, and 180 min as a contact time.

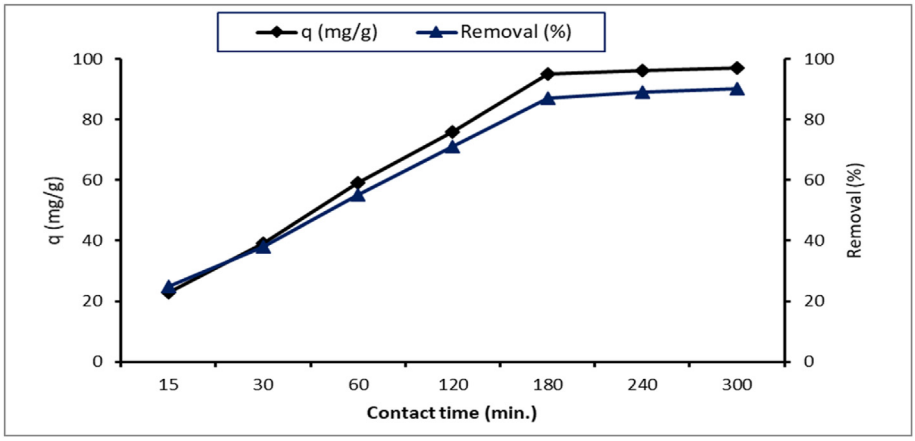

Fig. 14. Effect of contact time on the adsorptive removal of Cr (VI) using MOF/AmCS (0.5% AmCS) beads at a constant adsorbent dose of 0.1 g, Cr (VI) of 50 ppm 100/ml, pH = 2, adsorption temperature of 25 °C, and shaking speed of 150 rpm.

The investigation of the impact of pH variation on the adsorptive removal of Cr (VI) ions using MOF/AmCS beads with 0.5% AmCS was conducted within the pH range of 1–8, as depicted in Fig. 15. The experimental conditions involved the simultaneous maintenance of an adsorbent dose of 0.1 g, a Cr (VI) concentration of 50 ppm 100/ml, an adsorption temperature of 25 °C, a shaking speed of 150 rpm, and a contact duration of 180 min. The results indicate that an increase in pH from 1.0 to 2.0 led to a corresponding increase in both the adsorption capacity and removal efficiency (%) of Cr (VI). However, a subsequent increase in pH to 8.0 resulted in a decline in both parameters. The observed decrease in adsorption capacity at pH 1 in comparison to pH 2 can be attributed to the transformation of Cr (VI) species, leading to the formation of neutral H_2CrO_4 at pH levels of less than 2. The NH_2 groups that were positively protonated and the Cr (VI) ions that were negatively charged exhibited a slight attraction toward each other. The study conducted by Nomanbhay and Palanisamy (2005) showed a decrease in both adsorption capacity and percentage of Cr (VI) removal. Is it possible to obtain test samples that do not contain any adsorbent material? Is it possible for a portion of chromium to be eliminated through precipitation?

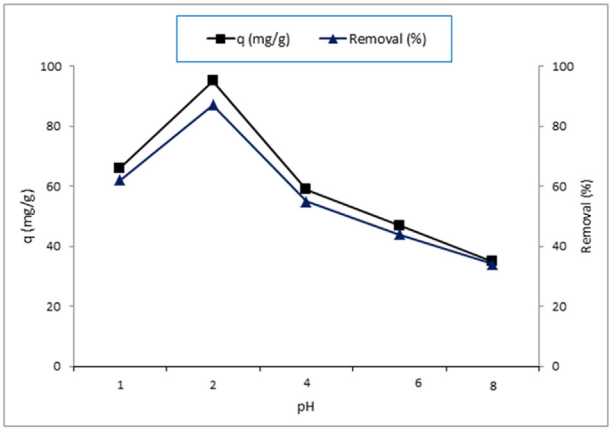

Fig. 15. Effect of pH variation on the adsorptive removal of Cr (VI) using MOF/AmCS (0.5% AmCS) beads at a constant adsorbent dose of 0.1 g, Cr (VI) of 50 ppm 100/ml, adsorption temperature of 25 °C, shaking speed of 150 rpm, and contact time of 180 min.

The MOF/AmCS bead surface had NH_2, COOH, and OH groups that were protonated at pH 2 to create a less negatively charged surface. As a consequence, the adsorptive removal of Cr would be improved by the stronger positive–negative charge attraction (VI). Moreover, the following equation can be used to describe the electrostatic interaction between negatively charged Cr (VI) ions and protonated species:

$$-NH3+ : -NH_3^+ + HCrO_4^- \rightarrow -NH_3^+ \ldots\ldots HCrO_4^- \quad (4)$$

Also, $-NH_3^+$ can bind with Cl^- (generated from hydrolysis of acidic HCl), and then the ion-exchange process takes place between $HCrO_4^-$ and Cl^- anions as presented in the following equation:

$$H_2CrO_4^- + 7H^+ + 3e^- \rightarrow Cr^{3+} + 4H_2O \quad (5)$$

It has been reported that the production of neutral H_2CrO_4 occurred at a pH of 2, concomitant with the reduction of certain negatively charged Cr (VI) ions to positively charged Cr (III) ions, as indicated by the equations. The decreased adsorption capacity observed at a pH of 1 in comparison to a pH of 2 may be ascribed to the transformation of Cr (VI) entities (7, 8). Consequently, a minimal attraction existed between the negatively charged Cr (VI) ions

and the positively protonated amine groups (NH3+). The study conducted by Sharma *et al.* (2017) showed a decline in both the adsorption capacity and the percentage of Cr (VI) removal.

$$H_2CrO_4^- + 7H^+ + 3e^- \rightarrow Cr^{3+} + 4H_2O \quad (6)$$

$$Cr_2O_7^{2-} + 14H^+ + 6e^- \rightarrow 2Cr^{3+} + 7H_2O \quad (7)$$

Conversely, an increase in pH of up to 8 results in a reduction of Cr (VI) removal from 87 to 34%, and a decrease in adsorption capacity from 97 to 35 mg/g. According to Sikder *et al.* (2014), the adsorbent surface experiences a decrease in positive charges due to the existence of an increased number of OH- ions in the adsorption medium.

The decrease in removal efficiency and adsorption capacity can be attributed to the attenuation of electrostatic interactions between the adsorbent and Cr (VI) ions of opposite charge.

Considering the circumstances, a pH value of 2 was designated as the optimal pH medium for subsequent adsorption experiments. Furthermore, the present study revealed congruent findings with prior research examined by Yang *et al.* (2022).

The adsorption mechanism can be examined by identifying the point of zero charge on the adsorbent surface. A pH over pH_{zpc} improves cation adsorption, while a pH below pH_{zpc} improves anion adsorption. Results indicate that the adsorbent has a pH of 2 (zpc). This indicates that the adsorbent surface had a neutral or zero charge at pH = 2. The study found no significant variance in the pH range of 3–8. However, the anionic environment can change the structure of Cr (VI). pH 2 (neutral for metal ions and adsorbent) was determined as the optimal pH (Zarei *et al.*, 2018).

3.6.4. Effect of initial Cr (VI) concentration

The study conducted experiments using different concentrations of Cr (VI) within the 10–200 ppm range while keeping all other adsorption parameters constant. The objective was to examine the influence of the initial Cr (VI) concentration on the adsorption process, as illustrated in Fig. 16.

The study showed a positive correlation between the concentration of Cr (VI) and the adsorption capacity, as the former increased from 10 to 200 ppm, the latter also exhibited a gradual increase from 19 to 132 mg/g. This hypothesis could be attributed to the failure to attain a state of adsorbent surface saturation at lower concentrations of 10 and 25 ppm. Conversely, with an increase in Cr (VI) concentration, there was a corresponding increase in adsorption capacity due to the progressive occupation of adsorption sites. The observed phenomenon could potentially be attributed to the resolution of the mass transfer resistance at the interface between the solid and liquid phases, as a result of the growth-promoting influences stemming from the concentration gradient. It is plausible that the dimensions of the adsorbent particles may also play a role in this process. The justification of potential mass transfer restrictions is deemed significant, as posited by Khan *et al.* (2022a, 2022b).

The findings indicated that diminished concentrations exhibited total elimination (100%) due to the surplus use of adsorbent in comparison to the

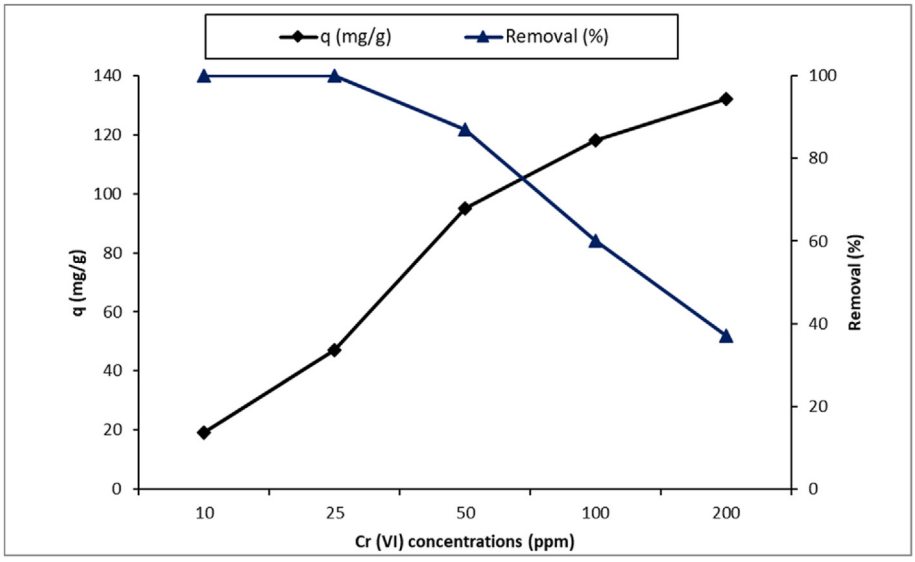

Fig. 16. Effect of Cr (VI) concentrations on the adsorptive removal of Cr (VI) using MOF/AmCS (0.5% AmCS) beads at a constant adsorbent dose of 0.1 g), pH of 2, adsorption temperature of 25 °C, shaking speed of 150 rpm, and contact time of 180 min.

requisite amount for the absorption of Cr (VI) ions. The complete removal of Cr (VI) ions was achieved due to the facile capture of these ions by the adsorption sites. At elevated concentrations of 100 and 200 ppm, the reduction in droplet percentage may be attributed to the limited availability of adsorption sites on the MOF/AmCS beads' surface. This is due to the saturation of these sites by specific concentrations of Cr (VI). Furthermore, it is plausible that heightened concentrations of Cr (VI) may result in the emergence of intensified intermolecular forces among solute molecules in both solid and bulk phases. Consequently, a reduced number of Cr (VI) ions were eliminated (%).

Exposure to concentration gradients of Cr (VI) of up to 200 ppm may cause the driving forces resulting from the concentration gradient to outweigh the resistance to mass transfer between the liquid and solid phases, which will increase the values of the adsorption capacity (Khan *et al.*, 2022a, 2022b).

3.6.5. Effect of adsorbent dose

The effects of the initial adsorbent dose variation on Cr (VI) removal (%) and the adsorption capacity under the same adsorption circumstances are shown in Fig. 17. The outcomes showed that as the dose of MOF/AmCS (0.5% AmCS) beads was increased from 0.05 to 0.3 g, their adsorption capacity steadily declined from 119 to 33 mg/g. This is due to the fact that according to the equation used to calculate adsorption capacity, adsorption capacity (q) is negatively proportional to the adsorbent dose. However, the dose was increased to 0.2 g and the removal (%) rose noticeably from 36 to 100%. These findings could be explained by the existence of more open adsorption sites, which would increase the adsorbent dose and, in turn, increase the elimination (%). However, as all Cr (VI) ions were completely removed (100%) using 0.2 g and 95% removed using 0.1 g, an additional rise in the adsorbent dose from 0.2 to 0.3 g does not affect the removal (%) (Khan *et al.*, 2022a, 2022b).

3.6.6. Effect of shaking speed

As shown in Fig. 18, the impact of shaking speed (rpm) on removal (%) and adsorption capacity was evaluated while maintaining all other adsorption conditions constant for a duration of more than 180 min. The obtained findings showed that the adsorption process is positively impacted by increasing the shaking speed to up to 150 rpm. The removal (%) increased steadily from 46 to 87% as a result, and the adsorption capacity rose from 49 to 95 mg/g. These results could be attributed to enhancing the distribution of solute in the bulk solution and improving the diffusion of Cr (VI) ions toward the bead's surface with increasing shaking speed to up to 150 rpm, resulting in the highest removal (%) with maximum adsorption capacity. Nevertheless, a further increase in the speed of up to 200 rpm increases the desorption tendency of Cr (VI), resulting from the deformation of the stationary film? If this is true then chromium is not strongly linked to the adsorbent which is opposite to the previous observations. Consequently, the removal (%) and adsorption capacity have decreased (Yang *et al.*, 2022).

3.6.7. Effect of medium temperature

As shown in Fig. 19, the influence of adsorption temperature on both elimination (%) and adsorption

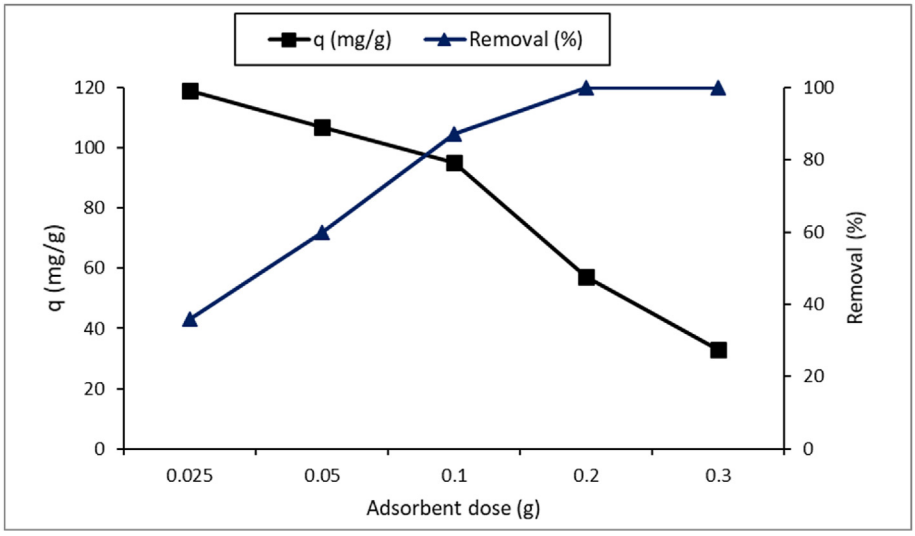

Fig. 17. Effect of adsorbent dose on the adsorptive removal of Cr (VI) using MOF/AmCS (0.5% AmCS) beads at a constant Cr (VI) of 50 ppm 100/ml, pH of 2, adsorption temperature of 25 °C, shaking speed of 150 rpm, and contact time of 180 min.

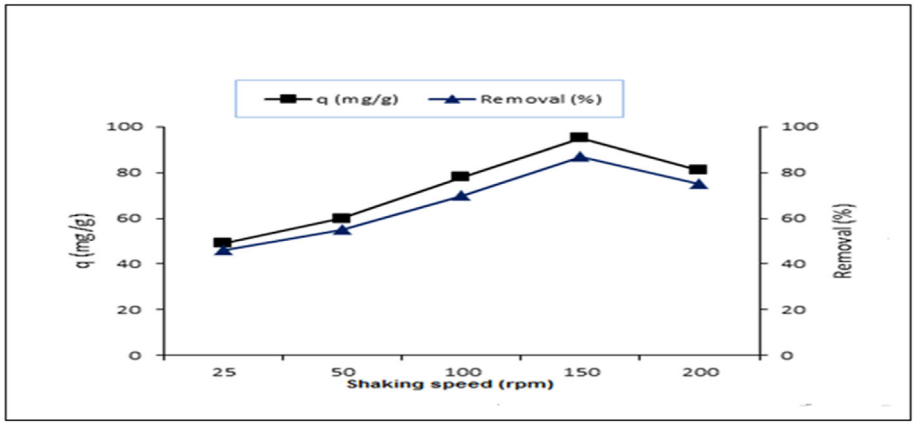

Fig. 18. Effect of shaking speed (rpm) on the adsorptive removal of Cr (VI) using MOF/AmCS (0.5% AmCS) beads at a constant adsorbent dose of 0.1 g, Cr (VI) of 50 ppm 100/ml, pH = 2, adsorption temperature of 25 °C, and contact time of 180 min.

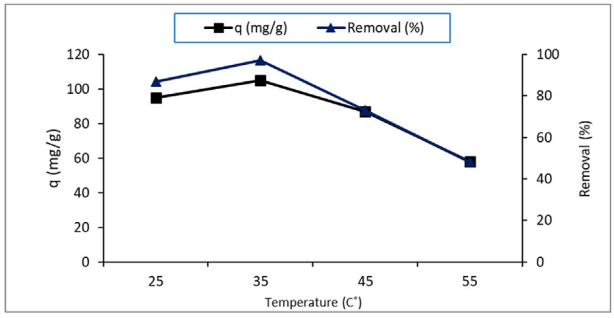

Fig. 19. Effect of temperature on the adsorptive removal of Cr (VI) using MOF/AmCS (0.5% AmCS) beads at a constant adsorbent dose of 0.1 g, Cr (VI) of 50 ppm 100/ml, pH = 2, shaking speed of 150 rpm, and contact time of 180 min.

capacity was investigated in the range of 25–55 °C. The outcomes showed that Cr (VI) ion removal (%) improved from 87 to 97%. However, as the temperature rose from 25 to 35 °C, the adsorption capacity grew from 95 to 105 mg/g. These could be brought on by greater segmental motion, which increases the diffusion rate of Cr (VI) ions over the external boundary layer of MOF/AmCS beads at higher temperatures of up to 35 °C. The adsorption process is affected and the removal (%) and adsorption capability decline as the temperature is raised further, up to 55 °C, which is related to the occurrence of maximal surface area in MOFs around 35 °C. The fluctuation in Cr (VI) removal seems to be consistent based on the surface area (Kar and Equeenuddin, 2019). These results could be explained by the fact that more energy is needed to improve Cr (VI) ion migration onto the surface of the bead. As a result, the likelihood of the Cr (VI) ions attaching diminishes, which triggers the desorption process and reduces the adsorption capacity and Cr (VI) removal (%). Adsorption in general is exothermic and it is reduced by the temperature! The initial increase in temperature is strange – it needs better justification with literature references (Yang *et al.*, 2022).

At pH 2 and 25 °C, the greatest adsorption capacity for removing Cr (VI) was 119 mg/g with an adsorbent dosage of 0.025 g. These values are significantly higher than the previously reported results of CS (93.6 mg/g) at pH 2 and temperature 40 °C (Wang *et al.*, 2016a, 2016b). Previous studies have shown that CS (78 mg/g) can effectively remove Cr (VI) (Schmuhl *et al.*, 2004).

3.7. Kinetic models

Kinetic models explore the rate at which adsorption occurs. By fitting experimental data to these models, we can gain insights into the rate-determining step and the type of adsorption:

(1) Pseudo-first-order model: assumes the rate of adsorption is proportional to the number of vacant sites on the MOF surface and the remaining adsorbate concentration. It suggests physisorption as the dominant mechanism.
(2) Pseudo-first-order and pseudo-second-order kinetic models were used to investigate the adsorption mechanism. The linear forms of pseudo-first-order and pseudo-second-order models:

$$ln\left(qe - qt\right) = lnqe - k1t \tag{8}$$

$$t \,/\, qt = 1 \,/\, \left(k2qe\,2\right) + t \,/\, qe \tag{9}$$

where k1 (min^{-1}) and k2 (g/mg/min) are the rate constants of pseudo-first-order and pseudo-second-order models, respectively, while qt (mg/g) and qe (mg/g) are the capacities at time t (min) and equilibrium. The values of k1, k2, and qe (qe cal) can be

determined from the intercept and the slope of the linear Eqs. (8) and (9). Moreover, to find the most reasonable model, the residual sum of squares (RSS) is commonly used and defined as

$$RSS = \sum i \left(qexp\, i - qmodel\, i\right)^2 \quad (10)$$

where qi exp and qi models are the experimental and model calculated values of the capacity qi. The smaller the RSS value, the more reasonable the model. The results are given. The correlation coefficient (R2) of the pseudo-second-order model was higher than that of the pseudo-first-order model, and the RSS value of the pseudo-second-order model was less than that of the pseudo-first-order model, which means that the fitting curve of the pseudo-second-order model was closer to the experimental points. These suggested that the pseudo-second-order model was more suitable for the adsorption of Cr (VI). Hence, the adsorption was mainly controlled by a chemical process (Fig. 20).

(1) Pseudo-second-order model: proposes that the rate of adsorption is controlled by the collision between adsorbate molecules and unoccupied sites. It often indicates chemisorption as the limiting step.
(2) Elovich model: accounts for a decreasing adsorption rate with time due to surface heterogeneity and blocking effects. It suggests chemisorption involving activation energy barriers (Fig. 21).

3.8. Adsorption isotherms

3.8.1. Langmuir isotherm

The Langmuir isotherm assumes monolayer adsorption with homogeneous binding sites and no interaction between adsorbed molecules. It suggests specific and energetically uniform binding, often indicating chemical adsorption (chemisorption) (Fig. 22).

3.8.2. Freundlich isotherm

This isotherm describes heterogeneous surfaces with a distribution of binding energies. It implies multilayer adsorption and is often associated with physisorption (Fig. 23).

3.8.3. Temkin isotherm

Temkin considers the decrease in binding enthalpy with surface coverage. It suggests an indirect interaction between adsorbate molecules and is indicative of chemisorption with lateral repulsion (Fig. 24).

3.9. Combined approach

By analyzing both isotherms and kinetic models, we can build a comprehensive picture of the adsorption mechanism:

(1) Dominant adsorption type: depending on the best fitting isotherm and kinetic model, we can identify the primary type of adsorption (physisorption or chemisorption).
(2) Interaction forces: specific isotherms like the Temkin suggest additional interactions such as electrostatic attraction or hydrogen bonding.
(3) Rate-determining step: kinetic models reveal whether diffusion, surface reaction, or both control the adsorption rate.
(4) Surface heterogeneity: Freundlich isotherm and Elovich model indicate a nonuniform surface with varying binding energies.

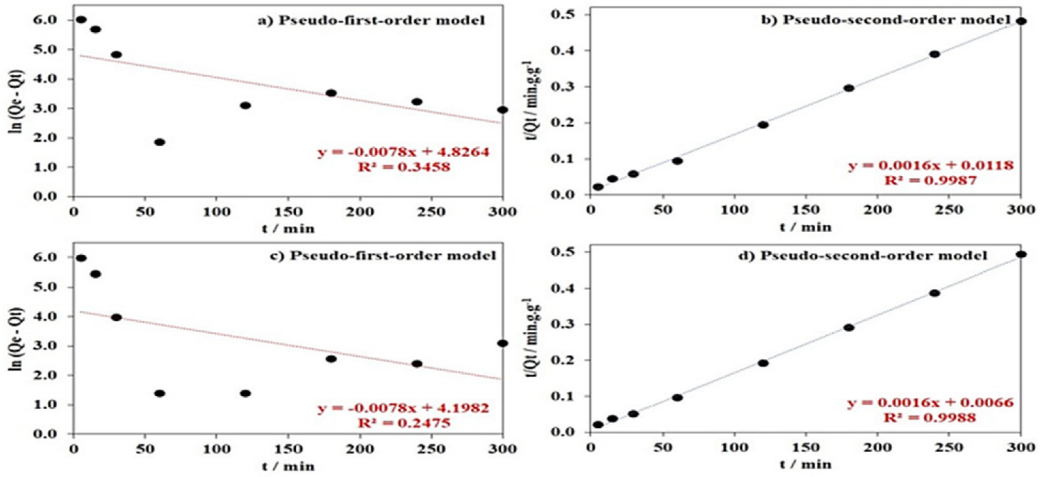

Fig. 20. (a,c) Pseudo-first- order and (b,d) pseudo-second order kinetic model for MOF adsorption.

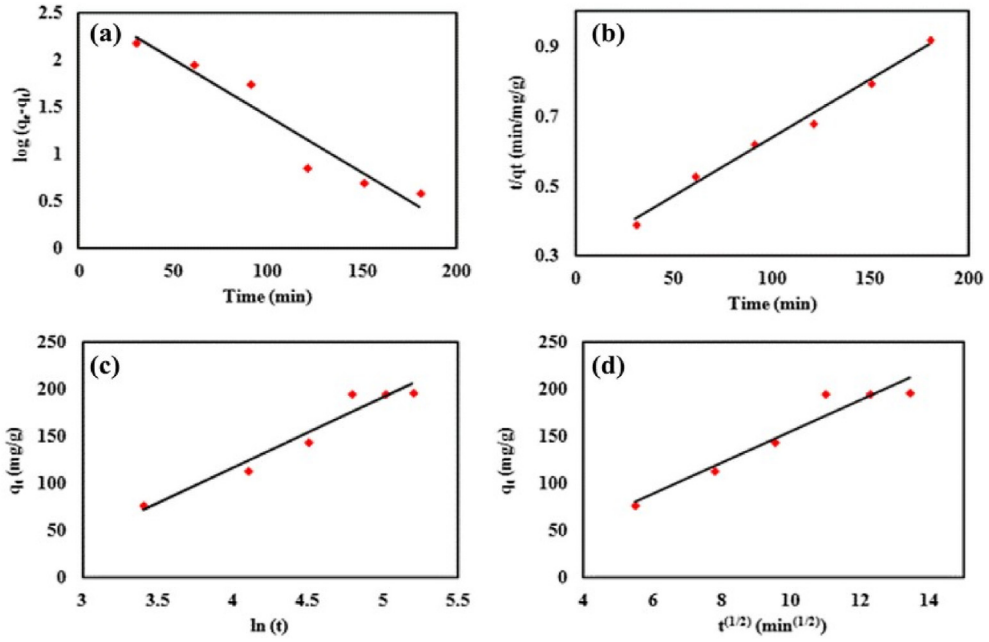

Fig. 21. Elovich model for MOF adsorption.

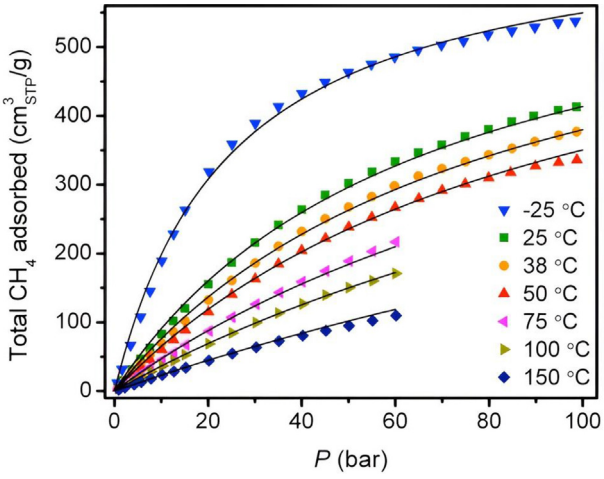

Fig. 22. Langmuir isotherm for MOF adsorption.

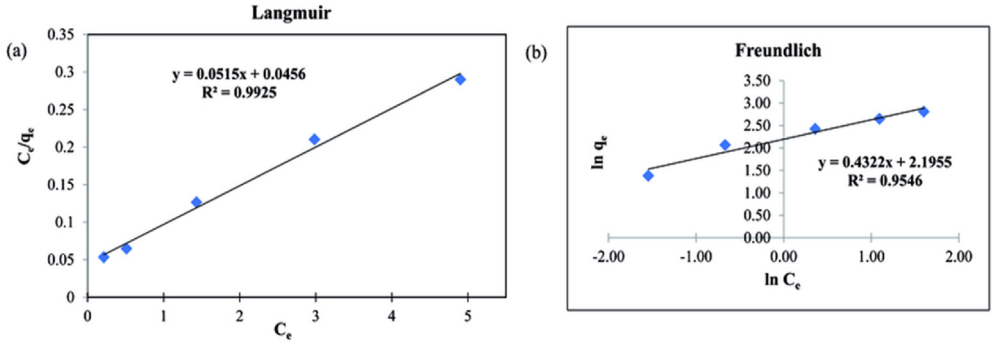

Fig. 23. (a) Langmuir and (b) Freundlich isotherms for MOF adsorption.

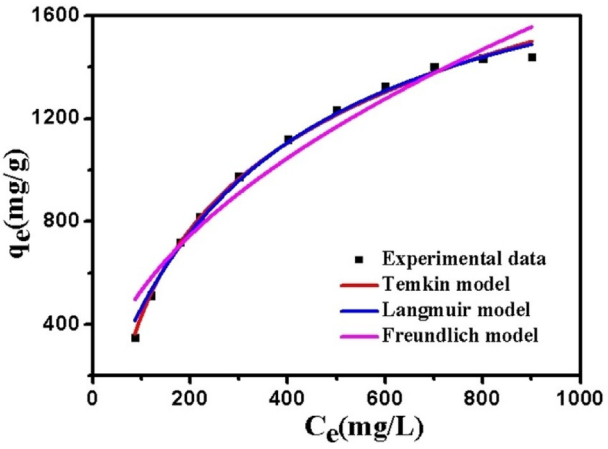

Fig. 24. Temkin isotherm for MOF adsorption.

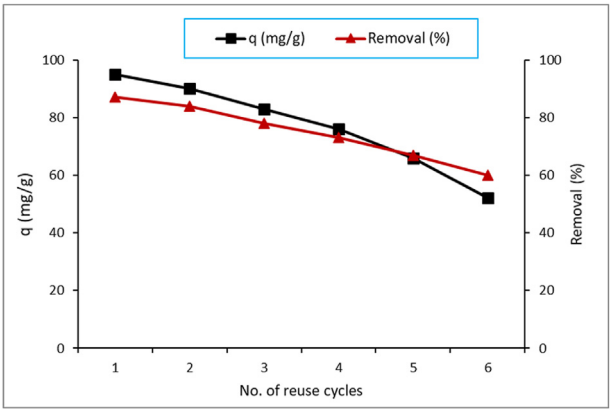

Fig. 25. Reusability cycles of the MOF/AmCS (0.5% AmCS) adsorbent at a constant adsorbent dose of 0.1 g, Cr (VI) of 50 ppm 100/ml, pH = 2, adsorption temperature of 25 °C, shaking speed of 150 rpm, and contact time of 180 min.

3.10. Example

Consider the adsorption of Cr (VI) onto a Zr-based MOF. Langmuir isotherm and pseudo-second-order kinetic model provide the best fit, suggesting specific and energetically uniform binding through strong chemisorption. This might involve the formation of stable metal–Cr (VI) complexes on the MOF's open metal sites.

3.11. Benefits of using models

(1) Predicting adsorption capacity and rate: models can help optimize MOF design and operating conditions for specific applications.
(2) Understanding interactions: we can gain insights into the nature and strength of binding forces between the MOF and the adsorbate.
(3) Developing new MOFs: model-based insights can guide the design of MOFs with tailored properties for targeted adsorption.

3.12. Reusability study

Economically speaking, the adsorbent's reusability is important because it directly impacts the production costs of the adsorbents. Adsorption–desorption experiments were carried out in this research to examine the prepared MOF/AmCS adsorbent's potential for reuse in the adsorption of Cr (VI). The results of these experiments are shown in Fig. 25. According to the findings, the MOF/AmCS adsorbent still possesses excellent adsorption characteristics after undergoing six repetitions of the adsorption–desorption cycle (60%) with a maximum adsorption capacity of 52 mg/g. This demonstrates how effectively removing Cr (VI) ions from their aqueous solution could be done while also being environmentally friendly and reusable.

3.13. Conclusion

This research successfully prepared and used new, inexpensive adsorbent hydrogel beads based on CS and its aminated derivatives to remove Cr (VI) ions from their aqueous solutions.

Chemical structures of the developed beads were described using FTIR, and their thermal stability was examined using thermogravimetric analysis. In comparison to the parent polymers, the findings showed that chemical cross-linking had increased the thermal stability of MOF/CS and MOF/AmCS beads. However, SEM analysis was used to find variations in surface morphology brought on by the formation of hydrogel beads.

By measuring the IEC, the amine content on the adsorbent's surface was determined (IEC). Because different amine groups were generated, it was discovered that the IEC values of the MOF/AmCS beads were greater than those of the MOF/CS beads. The IEC readings have risen as the AmCS concentrations have reached 0.5%. In addition, the swelling behavior of the developed beads under the MOF/AmCS condition was more pronounced than under the MOF/CS conditions, and it steadily increased with increasing AmCS concentrations of up to 0.5%.

Using batch adsorption experiments, the adsorption evaluation analysis of Cr (VI) ions was also carried out. A higher clearance (%) was discovered when CS, MOF/CS, and MOF/AmCS beads were used to compare the adsorptive removal of Cr (VI) ions. In comparison to the MOF/CS adsorbent (86%

and 93 mg/g using 1% CS) and Alg beads (18% and 15 mg/g), the MOF/AmCS adsorbent observed higher adsorption capacity values (87% and 95 mg/g using 0.5% AmCS).

The effects of CS and AmCS concentration, initial contact time, starting Cr (VI) concentration, pH, adsorbent dose, adsorption medium temperature, and shaking speed on the adsorption process were investigated (rpm). The inferences that can be drawn are the following:

(1) The removal (%) and adsorption capacity reached maximum values (87% and 95 mg/g) using 0.5% of AmCS.
(2) The equilibrium contact time for adsorption was 180 min.
(3) The maximum values of removal (%) and maximum adsorption capacity values were observed at a pH of 2.
(4) The highest removal (%) was estimated (100%) using 10 and 25 ppm of Cr (VI). At the same time, the maximum adsorption capacity was recorded using 200 ppm of Cr (VI).
(5) The maximum adsorption capacity was 119 mg/g using an adsorbent dose of 0.025 g, while the highest removal was 100% using 0.1 g of the prepared adsorbent beads.
(6) Maximum adsorption capacity and higher removal (%) values were recorded at 35 °C as the medium adsorption temperature (i.e. 109 mg/g and 97%).
(7) Maximum adsorption capacity and higher removal (%) values were recorded by conducting the adsorption experiments at 150 rpm.
(8) The MOF/AmCS adsorbent beads demonstrated good adsorption properties, with a removal rate exceeding 60% after six cycles, making them effective for removing toxic Cr (VI) ions from industrial wastewater.

Based on our findings, MOFs offer a potential pathway for the progression of wastewater treatment methodologies. Notwithstanding their potential, the use of MOFs in the context of wastewater treatment is still in its nascent phase, necessitating additional research to comprehensively comprehend and enhance their efficacy. The present article will center on the amalgamation and characterization of MOFs and their potential utilization in the remediation of industrial effluents.

3.14. Future work

Researchers may more readily and effectively model and simulate reticular systems with the use of computational tools, applications, and AI. No matter where they are in the world, researchers can now investigate and study MOFs, covalent organic frameworks, and other reticular structures thanks to technological breakthroughs.

Ethical clearance

The present manuscript is not submitted to more than one journal for simultaneous consideration. The submitted work is original and has not been published elsewhere in any form or language (partially or in full). The results are presented, honestly, and without fabrication, falsification, or inappropriate data manipulation. Authors adhere to discipline-specific rules for acquiring, selecting, and processing data. All authors agreed with the content that all gave explicit consent to submit and that they obtained consent from the responsible authorities at the institute/organization where the work was carried out before the work was submitted. The authors are responsible for the correctness of the statements provided in the manuscript. All authors certify that they have no affiliations with or involvement in any organization or entity with any financial interest or non-financial interest in the subject matter or materials discussed in this manuscript.

Funding statement

This research was carried out with the financial assistance of the European Union Fund under the ENI CBC Mediterranean Sea Basin Programme, Project B_A.2.1_0088_MED QUAD. The living lab. Smart Water Use Applications (SWUAP) was used to conduct the test of specimens.

Author contributions to idea and protocol design

Bassma M. Ali, Elen Emad, and Khalideh A.B. Alrawashdeh: conceptualization; Zainab Ali, Ragaa Ahmed, and Jalal A. Al-Tabbal: methodology; Rebhi A. Damseh and Kamel K. Al-Zboon: software; Petros Samaras, Bassma M. Ali, and Kareem Tonbol: validation; Bassma M. Ali, Elen Emad, and Kamel K. Al-Zboon: formal analysis; Kareem Tonbol and Bassma M. Ali: investigation; Yasser Dessouky: resources; Bassma M. Ali and Elen Emad: writing – original draft preparation; Petros Samaras: writing – review and editing; Rebhi A. Damseh: visualization; Kareem Tonbol: supervision; Rebhi A. Damseh: project administration; Yasser Dessouky: funding acquisition. All authors have read and agreed to the published version of the manuscript.

Declaration of Competing Interest

There are no conflicts of interest.

References

Abdelrazik, T.M., Valachová, K., Mohyeldin, M.S., Soltes, L., 2016. Free radical scavenger activity of cinnamyl chitosan schiff base. J. Appl. Pharmaceut. Sci. 6, 130–136.

Al-qudah, Y.H.F., Mahmoud, G.A., Abdel Khalek, M.A., 2014. Radiation crosslinked poly (vinyl alcohol)/acrylic acid copolymer for removal of heavy metal ions from aqueous solutions. J. Radiat. Res. Appl. Sci. 7, 135–145.

Amir Afshar, H., Ghaee, A., 2016. Preparation of aminated chitosan/alginate scaffold containing halloysite nanotubes with improved cell attachment. Carbohydr. Polym. 151, 1120–1131.

Bang, S.S., Pazirandeh, M., 1999. Physical properties and heavy metal uptake of encapsulated Escherichia coli expressing a metal binding gene (NCP). Escherichia coli 16, 489–499.

Bashir, M., Batool, M., Arif, N., Tayyab, M., Zeng, Y.J., Nadeem Zafar, M., 2023. Strontium-based nanomaterials for the removal of organic/inorganic contaminants from water: a review. Coord. Chem. Rev. 492 (February), 215286.

Cavka, J.H., Jakobsen, S., Olsbye, U., Guillou, N., Lamberti, C., Bordiga, S., Lillerud, K.P., 2008. Supplemental Cavka. J. Am. Chem. Soc. 130, 13850–13851.

Eldin, M.S.M., Soliman, E.A., Elzatahry, A.A.F., Elaassar, M.R., Elkady, M.F., Rahman, A.M.A., et al., 2012. Preparation and characterization of imino diacetic acid functionalized alginate beads for removal of contaminants from waste water: I. Methylene blue cationic dye model. Desalination Water Treat. 40, 15–23.

Garg, R., Sabouni, R., Alaamer, A., Alali, A., Al-Muqbel, D., Alqassem, H., Almazrooei, K., 2023. Recent development in metal-organic framework-based hybrid nanocomposites for pollutants remediation from wastewater: Challenges and opportunities. Environ. Technol. Innov. 32 (October), 103446.

Ihsanullah, Abbas, A., Al-Amer, A.M., Laoui, T., Al-Marri, M.J., Nasser, M.S., et al., 2016. Heavy metal removal from aqueous solution by advanced carbon nanotubes: Critical review of adsorption applications. Separ. Purif. Technol. 157, 141–161.

Kar, S., Equeenuddin, S.M., 2019. Adsorption of chromium (VI) onto natural mesoporous goethite: effect of calcination temperature. Groundwater Sustain. Dev. 9, 100250.

Khan, D.A., Banerji, A., Blumenthal, K.G., Phillips, E.J., Solensky, R., White, A.A., et al., 2022a. Drug allergy: a 2022 practice parameter update. J. Allergy Clin. Immunol. 150, 1333–1393.

Khan, U., Nairan, A., Gao, J., Zhang, Q., 2022b. Current progress in 2D metal–organic frameworks for electrocatalysis. Small Struct. 2200109, 2200109.

Kumari, S., Rath, P., Srei Hari Kumar, A., Tiwari, T.N., 2016. Removal of hexavalent chromium using chitosan prepared from shrimp shells. Afr. J. Biotechnol. 15, 50–54.

Lou, W., Li, J., Sun, W., Hu, Y., Wang, L., Neumann, R.F., et al., 2023. Screening Hoffman-type metal organic frameworks for efficient C2H2/CO2 separation. Chem. Eng. J. 452 (P2), 139296.

Mosquera, M.A., 2013. Simple isotherm equations to fit type I adsorption data. Fluid Phase Equil. 337, 174–182.

Ngah, W.S.W., Fatinathan, S., 2010. Pb(II) biosorption using chitosan and chitosan derivatives beads: equilibrium, ion exchange and mechanism studies. J. Environ. Sci. 22, 338–346.

Niṅā, I., Iorgulescu, M., Spiroiu, M.F., 2007. The adsorption of heavy metal ions on porous calcium alginate microparticles. Anal. Chem. I, 4–12.

Nirmal Kumar, J.I., Oommen, C., 2012. Removal of heavy metals by biosorption using freshwater alga Spirogyra hyalina. J. Environ. Biol. 33, 27–31.

Nomanbhay, S.M., Palanisamy, K., 2005. Removal of heavy metal from industrial wastewater using chitosan coated oil palm shell charcoal. Electron. J. Biotechnol. 8, 43–53.

Prasad, S., Yadav, K.K., Kumar, S., Gupta, N., Cabral-Pinto, M.M.S., Rezania, S., et al., 2021. Chromium contamination and effect on environmental health and its remediation: a sustainable approaches. J. Environ. Manag. 285 (February), 112174.

Reddy, D.H.K., Lee, S.M., 2013. Application of magnetic chitosan composites for the removal of toxic metal and dyes from aqueous solutions. Adv. Colloid Interface Sci. 201–202, 68–93.

Schmuhl, R., Krieg, H., Keizer, K., 2004. Adsorption of Cu(II) and Cr(VI) ions by chitosan: kinetics and equilibrium studies. WaterSA 27, 1–7.

Sikder, J., Chakraborty, S., Sharma, V., Drioli, E., 2014. Kinetic of lactic acid production from sugarcane juice using NCIM 2912. Asia-Pacific J. Chem. Eng. 9 (3), 374381. https://doi.org/10.1002/apj.1806.

Shafqat, S.S., Rizwan, M., Batool, M., Shafqat, S.R., Mustafa, G., Rasheed, T., Zafar, M.N., 2023. Metal organic frameworks as promising sensing tools for electrochemical detection of persistent heavy metal ions from water matrices: A concise review. Chemosphere 318 (January), 137920.

Sharma, S., Sourirajan, A., Dev, K., 2017 Jul. Role of Saccharomyces cerevisiae TAN1 (tRNA acetyltransferase) in eukaryotic initiation factor 2B (eIF2B)-mediated translation control and stress response. 3 Biotech. 7 (3), 223. https://doi.org/10.1007/s13205-017-0857-8. Epub 2017 Jul 4. PMID: 28677085; PMCID: PMC5496938.

Shriky, B., Mahmoudi, N., Kelly, A., Isreb, M., Gough, T., 2022. The effect of PEO homopolymers on the behaviours and structural evolution of Pluronic F127 smart hydrogels for controlled drug delivery systems. Colloids Surf. A Physicochem. Eng. Aspect. 645 (March), 128842.

Tambat, S.N., Sane, P.K., Suresh, S., Varadan, O.N., Pandit, A.B., Sontakke, S.M., 2018. Hydrothermal synthesis of NH2-UiO-66 and its application for adsorptive removal of dye. Adv. Powder Technol. 29, 2626–2632.

Wang, W., Kang, Y., Wang, A., 2013. One-step fabrication in aqueous solution of a granular alginate-based hydrogel for fast and efficient removal of heavy metal ions. J. Polym. Res. 20, 3.

Wang, K., Tao, X., Xu, J., Yin, N., 2016a. Novel chitosan-MOF composite adsorbent for the removal of heavy metal ions. Chem. Lett. 45, 1365–1368.

Wang, Y., Li, L.L., Luo, C., Wang, X., Duan, H., 2016b. Removal of Pb2+ from water environment using a novel magnetic chitosan/graphene oxide imprinted Pb2+. Int. J. Biol. Macromol. 86, 505–511.

Yang, F., Du, M., Yin, K., Qiu, Z., Zhao, J., Liu, C., et al., 2022. Applications of metal-organic frameworks in water treatment: a review. Small 18, 1–33.

Yoo, D.K., Lee, G., Mondol, M.M.H., Lee, H.J., Kim, C.M., Jhung, S.H., 2023. Preparation and applications of metal–organic frameworks composed of sulfonic acid. Coord. Chem. Rev. 474, 214868.

Zabochnicka-Świątek, M., Krzywonos, M., 2014. Potentials of biosorption and bioaccumulation processes for heavy metal removal. Pol. J. Environ. Stud. 23, 551–561.

Zafar, B., Shafqat, S.S., Zafar, M.N., Haider, S., Sumrra, S.H., Zubair, M., et al., 2022. NaHCO3 assisted multifunctional Co3O4, CuO and Mn2O3 nanoparticles for tartrazine removal from synthetic wastewater and biological activities. Mater. Today Commun. 33 (November), 104946.

Zarei, M., Djafarzadeh, N., Khadir, L., 2018. Removal of direct blue 129 from aqueous medium using surfactant-modified zeolite: a neural network modeling. Environ. Health Eng. Manag. 5, 101–113.